ACS Catalysis

pubs.acs.org/acscatalysis

Research Article

Thermodynamics and Kinetics of Molecular Hydrogen Adsorption and Dissociation on MXenes: Relevance to Heterogeneously Catalyzed Hydrogenation Reactions

Martí López, Ángel Morales-García, Francesc Viñes, and Francesc Illas*

Cite This: *ACS Catal.* 2021, 11, 12850−12857

Read Online

ACCESS | Metrics & More | Article Recommendations | Supporting Information

ABSTRACT: The interaction of molecular hydrogen with a series of 28 two-dimensional (2D) carbides and nitrides, known as MXenes, has been studied by means of periodic density functional calculations. This study shows that trends in atomic and molecular adsorption energies can be rationalized in terms of the electrostatic potential above the surface site and the Bader charge on the surface metal atoms. For all systems, molecular hydrogen is found to dissociate with almost negligible barriers, meaning that at low temperature the MXene surface will be passivated by adsorbed atomic hydrogen. The conditions at which the MXene surface is partly covered and, hence, able to participate in hydrogenation reactions are investigated by means of ab initio thermodynamics and phase diagrams derived from microkinetic simulations. The first provide the equilibrium conditions for a given H coverage on the MXene of interest, whereas the second provides the conditions at which a given configuration is reachable at the working conditions. For fast enough processes, both approaches necessarily lead to the same result, but this may differ when high energy barriers are involved, as it the case here for the H adatoms recombination step. With this suite, we show that Fe_2C, W_2N, and Mo_2C are promising hydrogenation catalysts. This work serves as a first step toward the rational design and implementation of MXene-based hydrogenation catalysts.

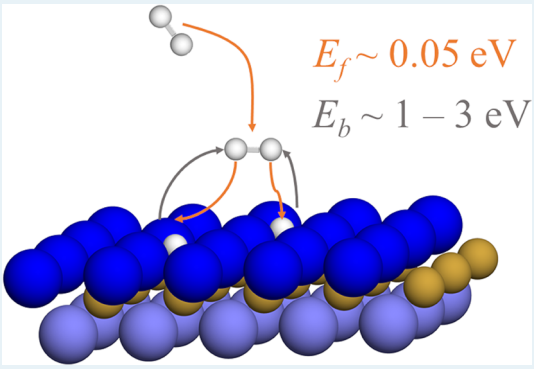

KEYWORDS: *MXenes, descriptor-based analysis, microkinetic simulations, hydrogenation, heterogeneous catalysis.*

1. INTRODUCTION

The new family of two-dimensional (2D) transition metal carbides and nitrides, termed MXenes, is attracting an increasing interest in materials science because of their new, tunable, and unexpected properties.[1−4] These new materials exhibit an outstanding performance in several applications involving batteries,[5,6] supercapacitors,[7] the electrochemical hydrogen evolution,[8,9] CO_2 abatement technologies,[10−12] heterogeneous catalysis,[13−17] and antibacterial activity,[18] just to name a few. MXenes are synthesized following a top-down approach starting from bulk MAX phases as precursors, where M is an early transition metal, A is typically Al or Si, and X is either C or N. In the MXene synthesis, the A component of the MAX phase is etched, generally using hydrofluoric acid (HF), with a subsequent sonication step to separate the as-produced 2D MXene layers.[19,20]

The thus-synthesized MXenes mainly exhibit the (0001) basal surface, which is structurally equivalent to the highly unstable and hard-to-prepare (111) surface of the corresponding bulk rock-salt transition metal carbides (TMCs) and nitrides (TMNs) single crystals.[21] Depending on the synthesis conditions, the MXene surfaces are covered with a variety of chemical species, most often -F, -O, and/or −OH. In the MXene literature, these surface terminations are usually denoted as T_x. Not surprisingly, the resulting MXene surface chemistry is heavily influenced by the synthesis conditions, that is, the MAX precursor, the solvent, and the used etchant agent.[22,23] Yet, recent work has shown that T_x terminations can be removed by combining high-temperature treatments with the subsequent hydrogenation of persistent -O groups,[10] which opens new avenues to the experimental study of the chemistry of bare MXene surfaces. Also, a new synthesis route has been reported using alkali metal halides as etchants that leads to MXenes with not so strongly bonded halide (T_x = -Cl, -Br) terminations. This constitutes another pathway toward pristine MXenes[24] and their use in numerous applications.[1,25−27]

Despite several promising applications.[25,28−32] and a salient ability to activate carbon dioxide (CO_2),[11,12] the rational selection criteria to choose a given MXene as a catalyst for a specific reaction, based for instance on descriptors determined

Received: July 13, 2021
Revised: September 9, 2021
Published: October 8, 2021

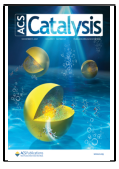

by their composition and/or electronic structure, remains elusive. The difficulty in finding reactivity descriptors for MXenes can be anticipated from their quite larger affinity for CO_2 compared with water (H_2O)[11,14] a surprising finding given the larger stability and lower chemical activity of CO_2 compared with H_2O.

To start addressing this challenge and to spur additional studies, we focus on the adsorption and dissociation of molecular hydrogen over 28 bare M_2X MXenes (M = Sc, Y, La, Ti, Zr, Hf, V, Nb, Ta, Cr, Mo, W, Mn, and Fe; X = C, N) by an interplay of first-principles calculations, ab initio thermodynamics, and microkinetic modeling. These tools allowed us to build not only phase diagrams corresponding to the most stable (more exergonic) surface hydrogen coverage situations but also to predict which of the possible stable surface structures can be kinetically reachable under realistic reaction conditions. In particular, we determine the conditions leading to the catalytically interesting region at which MXenes are not fully covered by atomic hydrogen and, hence, would efficiently operate in hydrogenation reactions, involving, for example, CO_2 hydrogenation, wherein a harmful greenhouse gas is converted to methanol or other useful chemicals while contributing to its abatement from the atmosphere,[33,34] or, to name another industrially relevant reaction, in ammonia synthesis.[14] In summary, we show here how combining thermodynamic and kinetic arguments could be useful to predict the conditions at which MXenes can be useful for hydrogenation reactions. We must point out that this constitutes a necessary but not sufficient condition. For the possible favorable cases, the particular hydrogenation reaction would need to be investigated in detail, whereas for the unfavorable ones, this can be directly skipped. Note also that the present analysis can be extended to other catalysts and to different environments.

2. COMPUTATIONAL DETAILS

Periodic density functional theory (DFT) calculations were carried employing the Vienna ab initio simulation package (VASP) code.[35] The broadly used Perdew−Burke−Ernzerhof (PBE) functional[36] was chosen to account for exchange and correlation effects, whereas dispersion interactions were included through Grimme's D3 approach.[37] The valence electron density was expanded using a plane-wave basis set with a cutoff kinetic energy of 415 eV, and the effect of the core electrons on the valence density was described through the projector augmented wave (PAW) method[38] as implemented in VASP.[39] The structural optimizations were considered converged when forces acting on atoms were below 0.01 eV $Å^{-1}$. The threshold for electronic energy convergence was set to 10^{-5} eV. The tetrahedron smearing method with Blöchl corrections was used in the calculations, with a 0.2 eV width, although the final total energies were always extrapolated to 0 K (no smearing). An optimal Γ-centered 5×5×1 **k**-point grid was used to sample the Brillouin zone for numerical integration in the reciprocal space. This computational setup, successfully used in previous works,[11,12,15] delivers converged results close to chemical accuracy (i.e., below ∼0.04 eV). For selected cases, spin polarization was accounted for, as described in more detail in the next section.

Adsorption sites for H and H_2 adsorption were sampled on a $p(3\times3)$ $M_2C(0001)$ surface supercell, see Figure 1, exposing ABC stacking of the atomic layers as in the parent MAX phases. The slabs are separated by a vacuum layer of at least 10 Å to avoid interaction between the periodically repeated images in the [0001] direction. The possible surface sites were sampled for both H adatoms and the H_2 molecule and initially placed ∼2 Å from the surface plane. In the case of H_2, several initial orientations were also considered. The corresponding structures were then fully relaxed. The adsorption energy, $E_{ads}^{H_x}$, for either the H adatoms (x = 1) or the H_2 molecule (x = 2) was estimated as

$$E_{ads}^{H_x} = E_{H_x/MXene} - \left(E_{MXene} + \frac{x}{2}E_{H_2}\right) \quad (1)$$

where $E_{H_x/MXene}$ is the energy of the surface with H* or H_2*, this is, x = 1 or 2, respectively, E_{MXene} is the energy of the pristine MXene surface, and E_{H_2} is the energy of H_2 in the gas phase. Note that E_H is obtained with respect to $\frac{1}{2}E_{H_2}$. With these conventions, the adsorption energy is negative for an exothermic process. The lists of E_{ads}^{H} and $E_{ads}^{H_2}$ values including zero-point energy (ZPE) contributions are reported in Tables S1 and S2 of the Supporting Information (SI), respectively.

The search for the transition states (TSs) of H_2 dissociation was performed using climbing-image nudged elastic band (CI-NEB) and dimer methods.[40,41] The thus located TS structures were characterized by frequency analysis ensuring that they exhibit just one imaginary frequency along the reaction pathways. The initial atomic configuration used to locate TS structures was the most stable adsorption configuration of H_2.

In addition, *ab initio* thermodynamics was employed to build phase diagrams following the method described by Reuter and Scheffler.[42,43] Details on the procedure can be found in a recent article by some of us dealing with the interaction between hydrogen and molybdenum carbides surfaces.[44] The thermodynamic study is complemented with microkinetic analysis,[45] where the Hertz-Knudsen equation is used to determine H_2 gas adsorption/desorption rates, in which transition-state theory was invoked to estimate the rates for the dissociation/recombination H_2* + * ↔ H* + H*

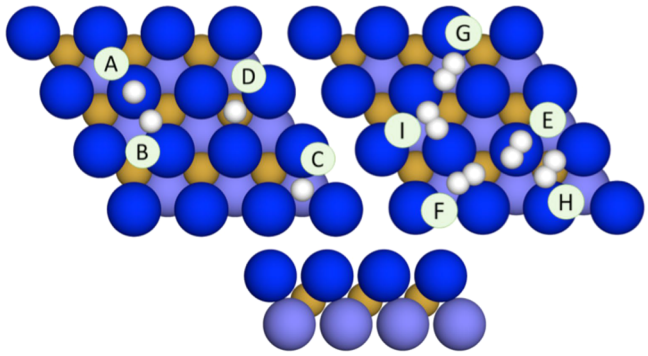

Figure 1. Top (upper images) and side (lower image) views of a M_2X (0001) surface $p(3\times3)$ supercell. Metal atoms at the top and bottom layers are represented by bright and light blue spheres, respectively, while C/N atoms are represented by light brown spheres, and H atoms are shown in white. The main high-symmetry surface sites for H atoms and perpendicular H_2 adsorption (left upper image) are top (A), bridge (B), hollow M (C), and hollow X (D), having either one M or X atom below, respectively. For H_2 adsorbed parallel to the $M_2X(0001)$ surface (right upper image), the sampled sites are top (E), XM bridge (F), hollow M (G), hollow X (H), and MM bridge (I).

https://doi.org/10.1021/acscatal.1c03150
ACS Catal. 2021, 11, 12850−12857

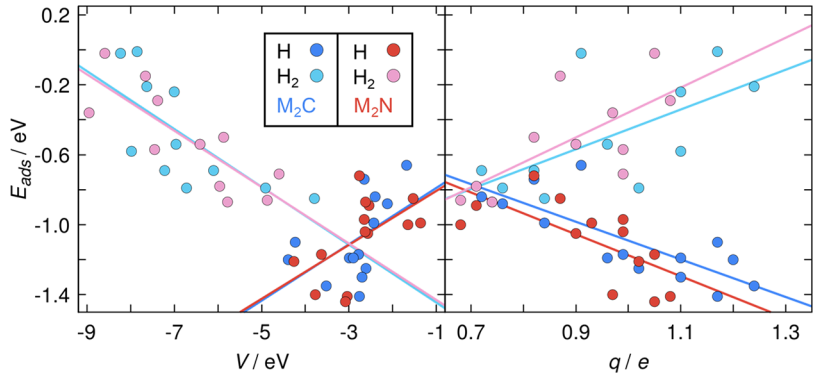

Figure 2. Trends in the adsorption energies of H* and H_2* with respect to the electrostatic potential, V, computed 1.5 Å above the surface plane (left), and with respect to the Bader charges, q, on the surface metal M atoms. Values for MCenes/MNenes are represented by blue/red circles, where the dark/light filled circles correspond to E_{ads}^{H} and $E_{ads}^{H_2}$, respectively. Linear fits and related statistical data are provided in Table S8 in the Supporting Information.

elementary surface reaction steps. The microkinetic simulations were carried out using the MKMCXX program,[46] employing an H_2 gaseous environment with an explored total pressure ranging from 100 μbar to 10 bar. Additional details and results on temperature ranges for a coverage of free sites from 0.2 to 0.6 monolayers (ML) are given in the SI.

3. RESULTS AND DISCUSSION

3.1. Atomic and Molecular Hydrogen Adsorption. We start with this section analyzing the atomic H adsorption on the different MXenes listed in Table S3 of the Supporting Information. In all cases, the most favorable adsorption site is hollow M site (H_M) —site C in Figure 1. There is the exception on La_2C, where hollow X (H_x) is preferred —site I in Figure 1. Geometry optimization starting with H placed above other sites such as bridge (B) and top (T) sites, labeled B and A in the leftmost panel of Figure 1, either lead to the described most stable situation or converged to situations with higher adsorption energies. Shortly, hollow sites accommodate H adatoms. Furthermore, spin-polarization-based calculations were explored for those cases previously reported to exhibit spin-polarized ground states such as Ti_2C,[47] Zr_2C,[47] Cr_2N,[48,49] Mn_2C,[50] or Mn_2N.[50] However, a systematic study of the different possible spin solutions using functionals not suffering from the well-known limitations of the GGA and GGA+U approaches is still lacking and out of the scope of the present study. Nevertheless, we observed that in most of the explored cases, spin polarization just slightly stabilizes bare MXene surfaces and has no effect on the energy of the H covered MXene. Consequently, it modifies E_{ads}^{H} by less than 0.1 eV. This is because, except for Fe_2X and Mn_2X, the presence of adsorbed hydrogen quenches the magnetic moments resulting in an electronic ground state which does not exhibit any spin polarization. Therefore, for the analysis of trends in subsequent sections, spin-polarized results can be safely neglected except, obviously, for the Fe_2X and Mn_2X MXenes. Attending to the results compiled in Table S3 of the Supporting Information, it is difficult to capture a trend in the adsorption energies. In general, the adsorption of atomic H runs between −0.66 and −1.44 eV depending on the MXene composition. The adsorption energy is slightly less exothermic when going down through the groups, except for Hf_2X where the adsorption is more favorable than for Zr_2X.

Regarding the H_2 molecular adsorption, see Table S4 of the Supporting Information, starting with H_2 perpendicular to the surface leads to a systematic physisorption with low $E_{ads}^{H_2}$ values up to −0.09 eV and H−H bond lengths around 0.76 Å, close to the H_2 bond length in vacuum of 0.75 Å. Conversely, stronger interactions in the range of −0.15 and −0.90 eV, see Table S4 of the Supporting Information, are observed for H_2 adsorption parallel to the surface above top (T) sites (indicated as E in the rightmost panel of Figure 1) locating the mass center of the molecule over such site. There are few cases (Sc_2C, Sc_2N, Ti_2C, Ti_2N, Mn_2C, and Mn_2N) with spontaneous dissociation upon relaxation. Other sites were tested, but the molecular dissociation was always achieved after optimization. Focusing on d^2-, d^3-, and d^4-metals, $E_{ads}^{H_2}$ is more exothermic moving along the series.

3.2. Molecular Hydrogen Dissociation and Recombination. In all cases, the energy barriers for molecular hydrogen dissociation, computed from the energy difference corresponding to the molecular adsorption configuration and that of the properly characterized transition state, are very low, see Table S5 of the Supporting Information. The molecular hydrogen tends to easily split into H* + H*. Only Zr_2C and Hf_2C feature energy barriers above 0.10 eV, and for the rest of MXenes, H_2 dissociation can be safely considered barrierless. The reaction energy computed as the difference between the energy of the MXene with two H* and that of the MXene with H_2* is compiled in Table S6 of the Supporting Information. The analysis of the results clearly indicates that the H* + H* scenario is energetically more favorable than the H_2* one.

To further inspect the dissociation reaction step, two different 2H* geometries have been explored, one with both H* at two H_M vicinal positions, which is the situation just after dissociation, and the other one with each H* at the farthest separated H_M sites in the supercell, which corresponds the most stable situation. The results listed in Table S7 indicate that there are no noticeable differences between them. Besides, comparing the adsorption energy per H adatom in any of the two (close or far) situations with the values corresponding to a single H adsorption, indicates that the lateral interactions between H* are negligible. Thus, we preliminarily conclude that MXenes readily dissociate hydrogen and the process does not strongly depend on the M or X components of the MXenes. A consequence of this reactivity is that the MXene surface will be readily covered by hydrogen and, hence,

https://doi.org/10.1021/acscatal.1c03150
ACS Catal. 2021, 11, 12850−12857

passivated, as the resulting system has no free active sites for other molecules that, eventually, could be hydrogenated. Therefore, determining the conditions at which the MXene surface is eventually partially covered becomes a real need for further applications in catalysis. This involves two well differentiated situations, namely, the conditions at which a thermodynamic equilibrium exists with the MXene surface partially covered and the conditions where such a situation is kinetically reachable during a reasonable contact time in between H_2 and the MXene catalyst. Obviously, this also involves determining which of the explored MXenes would exhibit the desired features.

3.3. Trends in Adsorption Energies. To rationalize the trends in E_{ads}, two possible descriptors were analyzed. These are the MXene electrostatic potential above the surface (V) and the surface metal charge (q). The V values were obtained using the Vaspview software[51] and computed at 1.5 Å above the surface Top and Hollow M positions. No significant variations in the trends were found for the V values at different heights. The net charges over the metal atoms were computed following Bader *Atoms-in-Molecules* analysis of the total electron density.[52] The results are summarized in Figure 2, while the calculated data appear in Tables S8 and S9 of the Supporting Information for V and q, respectively. We must point out that even if the correlation between E_{ads} and both descriptors is not good enough, they provide meaningful trends and a possible way to explain the differences in E_{ads} of H* and H_2* on MXenes.

Large negative V values indicate sites with more favorable H adsorption and likely stronger Pauli repulsion for molecular H_2* species.[53] The same view is obtained from the MXene surface metal Bader charge, q, thus providing another useful descriptor as shown on related transition metal carbide surfaces.[54,55] This descriptor shows that the more oxidized the metal, the stronger E_{ads} of H, while negative q would favor H_2 physisorption because of the enhancement of dispersion interactions. The charge on the metal sites where H* and H_2* present comparable binding strengths and, hence, can be optimal for hydrogenation purposes, is around 0.7−0.8 e, corresponding to Cr, Mo, W, Mn, and Fe, see Table S9. All in all, the two descriptors provide consistent trends and help rationalizing the opposing slopes for H* and H_2* adsorption. The data corresponding to the linear fits for the plots in Figure 2 are reported in Table S10 of the Supporting Information. The mean absolute errors (MAEs) between the linear fits and the calculated points in Figure 2 are comparable for the two descriptors and in all cases below 0.20 eV, which is an accepted value for the accuracy of DFT at the GGA level. The linear fits relating adsorption energies and either V or q in Table S10 display a clear, yet not quantitative, trend. This provides an indication that these descriptors can be used to make educated guesses of hydrogen adsorption energies in other MXenes and, perhaps, of other adsorbates, although this remains to be proven.

Before ending this section, we want to highlight that, while the hydrogen bonding at the explored MXenes surfaces cannot be described as governed by electrostatics, the electrostatic potential acts as the driving force determining the active sites as shown by some of us for atomic H at several low Miller indexes surfaces Pt surfaces.[53] Thus, the electrostatic potential initiates the interaction, but once the hydrogen is anchored, the short-range interactions govern the chemical bond.

3.4. Thermodynamic versus Kinetic Phase Diagrams. The analysis of the results corresponding to the atomic and molecular adsorption of hydrogen discussed in the previous sections reveals that the MXenes with M = Cr, Mo, W, Mn, and Fe, have comparable adsorption energies for H and H_2 and are, thus, promising good hydrogenation catalysts. This information is already found from the V and q descriptors as pinpointed in Figure 2, as these MXenes are those close to the crossover between the lines with opposing slope. Nevertheless, the easy dissociation of molecular hydrogen and the large exothermicity of this elementary step for most of the MXenes indicate that the MXene surface will be readily covered by atomic hydrogen thus impeding hydrogenation reactions, as no free sites would be available to the molecule to be hydrogenated. Thus, it is important to explore the conditions where the MXene surface is only partially covered by H* atoms. The atomistic thermodynamics formalism of Reuter et al.[42,43] has been used to build a phase diagram with the relative free energy of well-ordered phases as a function of H* coverage. In Figure 3 we present the phase diagram for W_2N

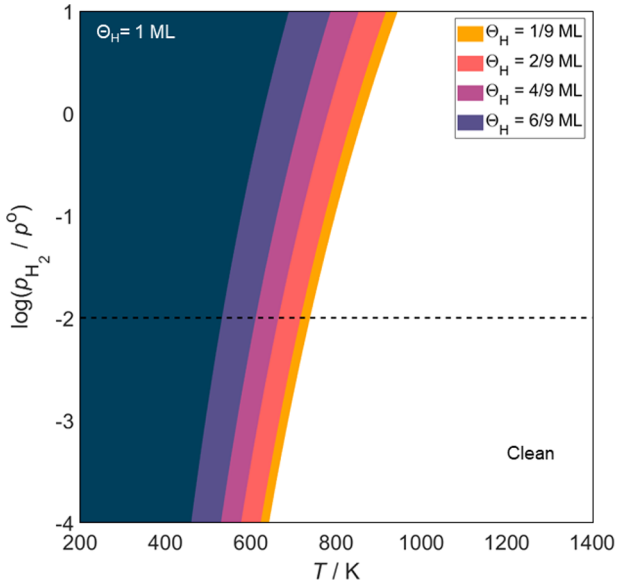

Figure 3. Thermodynamic phase diagram as a function of T and p_{H_2} for W_2N (0001) MXenes including different atomic hydrogen coverages, θ_H. It runs from 0 to 1 monolayer (ML). The black dashed line corresponds to a reference p_{H_2} of 10 mbar.

taken as a representative of this set of possibly good candidates. Indeed, Figure 3 shows that even at relatively high H_2 partial pressure, the surface is partly covered or even clean at temperatures in the 400−600 K and, therefore, provides support to the hypothesis that these MXenes are likely to perform well in hydrogenation reactions. For comparison, the phase diagrams for Fe_2C, a second good candidate for hydrogenation catalyst, and also for Ti_2C and Ti_2N, likely to be easily deactivated, are reported in section S5 of the Supporting Information. Note that the phase diagrams for Ti_2C and Ti_2N exhibit an abrupt transition from fully occupied to bare surface which, as predicted, indicates that these represent the worst scenario for hydrogenation.

The ab initio thermodynamic approach is undoubtedly extremely useful to determine the relative thermodynamic stability of surfaces with different surface coverage. However,

https://doi.org/10.1021/acscatal.1c03150
ACS Catal. 2021, 11, 12850−12857

being a purely thermodynamic approach, it does not incorporate any kinetic consideration. For processes reaching the thermodynamic equilibrium in a very fast way, the approach will provide meaningful information. However, for process involving rather large barriers, as is the case for H* + H* recombination leading to H_2* which eventually desorbs, the kinetic aspects may introduce noticeable changes. Here, one must advert that the kinetic aspects are not especially relevant for H_2 dissociation because the activation barriers are always very low. However, their role is crucial in the recombination step leading to H_2 formation that eventually desorbs, thus freeing some surface sites. The complete set of energy barriers for the dissociation and recombination steps is included in Table S5 of the Supporting Information.

To take a step forward in this direction, we propose a new approach in which microkinetic simulations are used to build kinetic, instead of thermodynamic, phase diagrams aiming to determine the reaction temperature, T, and hydrogen partial pressure, p_{H_2} at which the $M_2X(0001)$ MXene surfaces will be partially covered. The microkinetic simulations make use of rates derived either from kinetic gas theory via the Hertz-Knudsen equation (H_2 adsorption and desorption) or from statistical thermodynamics via transition-state theory (H_2* dissociation and H* + H* recombination) as described in detail in Section S1 of the Supporting Information. The results for Ti_2N, Ti_2C, Fe_2C, and W_2N at different p_{H_2} are displayed in Figure 4. This choice is to include MXene with an excessive

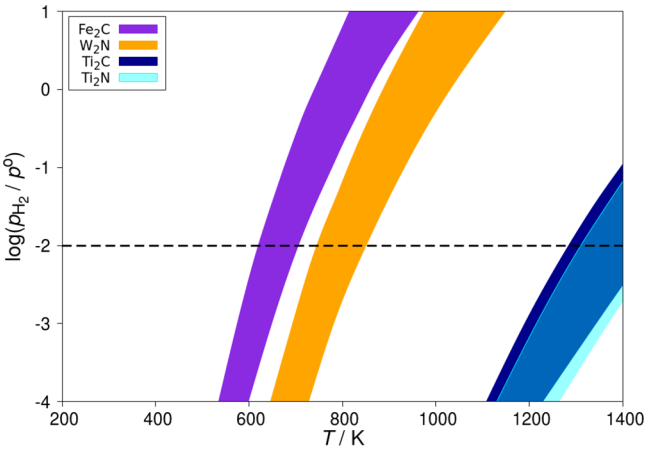

Figure 4. Kinetic phase diagrams as a function of T and p_{H_2} for Fe_2C, W_2C, Ti_2C, and Ti_2N MXenes derived from microkinetic simulations. The colored regions denote conditions with a coverage of free sites between 0.2 (rightmost line of each region) and 0.6 ML (leftmost line of each region), while the rest is covered with H adatoms. Notice that the overlapping region between Ti_2C (dark blue) and Ti_2N (cyan) is colored in light blue. The black dashed line corresponds to a reference p_{H_2} of 10 mbar.

affinitive for H adatoms (Ti_2N and Ti_2C) and two of the aforementioned promising MXene catalysts for hydrogenation reactions (Fe_2C and W_2N). These MXenes do also constitute limiting cases for H_2 formation barriers by H* + H* recombination.

The highlighted regions in Figure 4 denote situations where the coverage of free sites is 0.2−0.6 monolayers (ML) and, consequently, with a H* coverage in the range of 0.4−0.8 ML, see section S11 of the Supporting Information. Notice that the sum of coverages of the possible surface species, $\theta_* + \theta_H + \theta_{H_2} = 1$, and no population of H_2* moieties is detected in the microkinetic simulations. Despite the high upper limit for H* coverage of 0.8 ML, the thermodynamics and kinetics of hydrogen recombination were estimated at the dilute limit, that is at low H* coverage. This is justified because lateral interactions between adsorbed hydrogen atoms were found to be negligible, see Table S7 of the Supporting Information. In line with the predictions of the descriptor-based analysis, the smallest barriers correspond to Fe_2C and W_2N, whereas Ti_2N has one of the largest H_2 formation barriers, see Section S5 in the Supporting Information. Besides, Ti_2C is included because it can be considered a prototypical MXene with reactivity close to the first synthesized, and nowadays, broadly used Ti_3C_2 MXene.[21] We note that the highest recombination barrier corresponds to Hf_2C, yet it is excessively high to be of practical use. In fact, in the presence of oxygen, Hf_2C decomposes into CO_2 and the corresponding bulk HfC before reaching the target surface coverage conditions.[56,57]

From the microkinetic analysis for bare Ti-based MXenes, we observe that H adsorption is strong enough to keep the surface fully passivated even above 1200 K for most p_{H_2} conditions, an upper bound for Ti_2X thermal stability.[58] Therefore, bare Ti_2C and Ti_2N MXenes will presumably not be good hydrogenation catalysts, although the presence of other surface species such as -O or -F might change this conclusion. Indeed, Persson et al.[10] used 8 mbar H_2 at 973 K to experimentally clean Ti_3C_2 surfaces, hydrogenating the surface -O moieties, close to the values for Ti_2C obtained here, see Figure 4. This also indicates that the working temperature can be lowered using smaller p_{H_2}. Interestingly, at p_{H_2} = 10 mbar, bare Fe_2C displays a range of temperatures of 620−707 K to meet the target coverages. As Fe is one of the most common and affordable metals on the Earth's crust, Fe-containing carbide MXenes are good candidates for hydrogenation reactions. Since MXene thickness has little influence on their surface chemistry,[21] Fe_2C and Fe_2C_3 MXenes probably exhibit similar reactivities toward H_2. Note, however, that these MXenes have not been experimentally synthesized yet, and that the effect of surface terminations should be explored.

Although W_2N is slightly worse than Fe_2C, with working temperatures ranging from 745 to 852 K at p_{H_2} = 10 mbar, it has already been synthesized.[59] Here it is worth comparing the predictions from the ab initio thermodynamics and the kinetic phase diagrams. Qualitatively, both approaches lead to a similar description in the sense that heating at rather high temperatures will lead to a partial coverage of atomic hydrogen and, hence, to good candidates for hydrogenation reactions. However, the predicted temperature at which the W_2N surface starts to display free sites is significantly larger when kinetic phase diagrams are employed; ∼700 K versus ∼400 K as predicted from the ab initio thermodynamics.

The analysis of the kinetic phase diagrams highlights the role of the energetic barrier for H_2 formation in determining the conditions for MXenes to be active hydrogenation catalysts and these are significantly different from those predicted from thermodynamic considerations only. Considering the thermal stability limit for MXenes, a threshold on the H_2 formation barrier of ∼2.50 eV can be set, based on the fact that Zr_2C (2.56 eV) has a range of temperatures between 1120 and 1259 K at 10 mbar of H_2, already above typical MXene decomposition temperatures.

https://doi.org/10.1021/acscatal.1c03150
ACS Catal. 2021, 11, 12850−12857

4. CONCLUSIONS

A systematic theoretical study has been presented on the basis of DFT-D3 calculations for a number of MXene surface models. We disclosed here the trends in the interaction between H and H_2 with the M_2X materials by analyzing their description through the electrostatic potential above the surface and the surface metal Bader charges. For these two descriptors, the trends in H and H_2 adsorption are opposite, the former being modulated by electrostatic factors and the latter governed by dispersive forces.

Further analysis with ab initio thermodynamics and microkinetic modeling approaches shows that Fe_2C, W_2N, and Mo_2C are promising hydrogenation catalysts in the sense that the conditions at which the surface of these MXenes is only partially covered by hydrogen, are within the range of thermal stability of these materials and are similar to those used commonly in the chemical industry. Nevertheless, it is important to point out that the predictions from ab initio thermodynamics lead to temperature conditions milder than those predicted from the newly presented kinetic phase diagrams that account for the energy barriers required for atomic hydrogen to recombine and desorb. These differences are likely to be important in other systems as well where the thermodynamic equilibrium will take longer than the chemical reactions that the material of interest is supposed to catalyze.

We note that, in agreement with the predictions in the present work, W_2N was indeed predicted as a potential catalyst for ammonia synthesis,[14] which is an important industrial hydrogenation reaction. In addition, our results likely hold for MXenes involving more atomic layers, as thickness usually bears little effect on MXene surface chemistry.[21] Besides, the predictions made here are to be coupled with the reported favorable CO_2 activation on several MXenes[10,12] and experimentally confirmed in some cases, so as to find prospect catalysts for catalytic CO_2 reduction.

We hope our observations and specific combination of computational techniques foster further research on the subject and contribute to the elaboration of a quantitative, comprehensive, and data-driven theory of MXene-based catalysis. In particular, the present study calls for future experiments and further studies inspecting surface termination effects.

■ ASSOCIATED CONTENT

Supporting Information

The Supporting Information is available free of charge at https://pubs.acs.org/doi/10.1021/acscatal.1c03150.

Microkinetic modeling and kinetic phase diagrams. Atomic and molecular hydrogen adsorption energies. Molecular hydrogen dissociation energy barrier and reaction energy. Descriptors. Phase diagrams for Fe_2C, Ti_2C and Ti_2N and selected results for kinetic phase diagrams (PDF)

■ AUTHOR INFORMATION

Corresponding Author

Francesc Illas − *Departament de Ciència de Materials i Química Física & Institut de Química Teòrica i Computacional (IQTCUB), Universitat de Barcelona, Barcelona 08028, Spain;* orcid.org/0000-0003-2104-6123; Email: francesc.illas@ub.edu

Authors

Martí López − *Departament de Ciència de Materials i Química Física & Institut de Química Teòrica i Computacional (IQTCUB), Universitat de Barcelona, Barcelona 08028, Spain*

Ángel Morales-García − *Departament de Ciència de Materials i Química Física & Institut de Química Teòrica i Computacional (IQTCUB), Universitat de Barcelona, Barcelona 08028, Spain;* orcid.org/0000-0003-0491-1234

Francesc Viñes − *Departament de Ciència de Materials i Química Física & Institut de Química Teòrica i Computacional (IQTCUB), Universitat de Barcelona, Barcelona 08028, Spain;* orcid.org/0000-0001-9987-8654

Complete contact information is available at: https://pubs.acs.org/10.1021/acscatal.1c03150

Notes

The authors declare no competing financial interest.

■ ACKNOWLEDGMENTS

The authors thanks Dr. Federico Calle-Vallejo for many discussions and remarks. Financial support was provided by Spanish *Ministerio de Ciencia, Innovación y Universidades* (MICIUN) through grants RTI2018-095460-B-I00 and *María de Maeztu* MDM-2017-0767 and, in part, by *Generalitat de Catalunya* 2017SGR13 grant. We thank *Red Española de Supercomputación* (*RES*) for supercomputing resources (projects QCM-2018-1-0009, QCM-2018-3-0015). A.M.G. thanks MICIUN for a *Juan de la Cierva* (IJCI-2017-31979) research contract. M.L. thanks *Universitat de Barcelona* for an APIF predoctoral contract.

■ REFERENCES

(1) Anasori, B.; Lukatsaya, M. R.; Gogotsi, Y. 2D Metal Carbides and Nitrides (MXenes) for Energy Storage. *Nat. Rev. Mater.* **2017**, *2*, 16098.

(2) Chaudhari, N. K.; Jin, H.; Kim, B.; Baek, D. S.; Joo, S. H.; Lee, K. MXene: An Emerging Two-Dimensional Material for Future Energy Conversion and Storage Applications. *J. Mater. Chem. A* **2017**, *5*, 24564−24579.

(3) Gogotsi, Y.; Anasori, Y. The Rise of MXenes. *ACS Nano* **2019**, *13*, 8491−8494.

(4) VahidMohammadi, A.; Rosen, J.; Gogotsi, Y. The World of Two-Dimensional Carbides and Nitrides (MXenes). *Science* **2021**, *372*, eabf1581.

(5) Er, D.; Li, J.; Naguib, M.; Gogotsi, Y.; Shenoy, V. B. Ti_3C_2 MXene as a High Capacity Electrode Material for Metal (Li, Na, K, Ca,) Ion Bateries. *ACS Appl. Mater. Interfaces* **2014**, *6*, 11173−11179.

(6) Liang, X.; Garusch, A.; Nazar, L. F. Sulfur Cathodes Based on Conductive MXene Nanosheets for High-Performance Lithium-Sulfur Batteries. *Angew. Chem., Int. Ed.* **2015**, *54*, 3907−3977.

(7) Wang, X.; Kajiyama, S.; Iinuma, H.; Hosono, E.; Oro, S.; Moriguchi, I.; Okubo, M.; Yamada, A. Pseudocapacitance of MXene Nanosheets for High-Power Sodium-Ion Hybrid Capacitors. *Nat. Commun.* **2015**, *6*, 6544.

(8) Handoko, A. D.; Fredrickson, K. D.; Anasori, B.; Convey, K. W.; Johnson, L. R.; Gogotsi, Y.; Vojvodic, A.; She, Z. W. Tuning the Basal Plane Functionalization of Two-Dimensional Metal Carbides (MXenes) to Control Hydrogen Evolution Activity. *ACS Appl. Energy Mater.* **2018**, *1*, 173−180.

(9) Seh, Z. W.; Fredrickson, K. D.; Anasori, B.; Kibsgaard, J.; Strickler, A. L.; Lukatskaya, M. R.; Gogotsi, Y.; Jaramillo, T. F.; Vojvodic, A. Two-Dimensional Molybdenum Carbide (MXene) as an

Efficient Electrocatalyst for Hydrogen Evolution. *ACS Energy Lett.* **2016**, *1*, 589−594.
(10) Persson, I.; Halim, J.; Linds, H.; Hansen, T. W.; Wagner, J. B.; Näslund, L.; Darakchieva, V.; Palisaitis, J.; Rosen, J.; Persson, P. O. Å. 2D Transition Metal Carbides (MXenes) for Carbon Capture. *Adv. Mater.* **2018**, *31*, 1805472.
(11) Morales-Salvador, R.; Morales-García, Á.; Viñes, F.; Illas, F. Two-Dimensional Nitrides as Highly Efficient Potential Candidates for CO_2 Capture and Activation. *Phys. Chem. Chem. Phys.* **2018**, *20*, 17117−17124.
(12) Morales-García, Á.; Fernández-Fernández, A.; Viñes, F.; Illas, F. CO_2 abatement using two-dimensional MXenes carbides. *J. Mater. Chem. A* **2018**, *6*, 3381−3385.
(13) Li, N.; Chen, X.; Ong, W. J.; MacFarlane, D. R.; Zhao, X.; Cheetham, A. K.; Sun, C. Understanding of Electrochemical Mechanisms for CO_2 Capture and Conversion into Hydrocarbon Fuels in Transition-Metal Carbides (MXenes). *ACS Nano* **2017**, *11*, 10825−10833.
(14) Gouveia, J. D.; Morales-García, Á.; Viñes, F.; Gomes, J. R. B.; Illas, F. Facile Heterogeneously Catalyzed Nitrogen Fixation by MXenes. *ACS Catal.* **2020**, *10*, 5049−5056.
(15) Gouveia, J. D.; Morales-García, Á.; Viñes, F.; Gomes, J. R. B.; Illas, F. MXenes as Promising Catalysts for Water Dissociation. *Appl. Catal., B* **2020**, *260*, 118191.
(16) Wei, H.; Jiang, Q.; Ampelli, C.; Chen, S.; Perathoner, S.; Liu, Y.; Centi, G. Enhancing N_2 Fixation Activity by Converting Ti_3C_2 MXenes Nanosheets to Nanoribbons. *ChemSusChem* **2020**, *13*, 5614−5619.
(17) Slot, T. K.; Natu, V.; Ramos-Fernandez, E. V.; Sepúlveda-Escribano, A.; Barsoum, M.; Rothenberg, G.; Shiju, N. R. Enhancing catalytic epoxide ring-opening selectivity using surface modified $Ti_3C_2T_x$ MXenes. *2D Mater.* **2021**, *8*, 035003.
(18) Rasool, K.; Helal, M.; Ali, A.; Ren, C. E.; Gogotsi, Y.; Mahmoud, K. A. Antibacterial Activity of $Ti_3C_2T_x$ MXene. *ACS Nano* **2016**, *10*, 3674−3684.
(19) Naguib, M.; Mashtalir, O.; Carle, J.; Presser, V.; Lu, J.; Hultman, L.; Gogotsi, Y.; Barsoum, M. W. Two-Dimensional Transition Metal Carbides. *ACS Nano* **2012**, *6*, 1322−1331.
(20) Naguib, M.; Kurtoglu, M.; Presser, V.; Lu, J.; Niu, J.; Heon, M.; Hultman, L.; Gogotsi, Y.; Barsoum, M. W. Two-Dimensional Nanocrystals Produced by Exfoliation of Ti_3AlC_2. *Adv. Mater.* **2011**, *23*, 4248−4253.
(21) Morales-García, Á.; Mayans-Llorach, M.; Viñes, F.; Illas, F. Thickness Biased Capture of CO_2 on Carbide MXenes. *Phys. Chem. Chem. Phys.* **2019**, *21*, 23136−23142.
(22) Halim, J.; Cook, K. M.; Naguib, M.; Eklund, P.; Gogotsi, Y.; Rosen, J.; Barsoum, M. W. X-Ray Photoelectron Spectroscopy of Select Multi-layered Transition Metal Carbides (MXenes). *Appl. Surf. Sci.* **2016**, *362*, 406−417.
(23) Xie, Y.; Kent, P. R. Hybrid Density Functional Study of Structural and Electronic Properties of Functionalized $Ti_{n+1}X_n$ (X = C, N) Monolayers. *Phys. Rev. B: Condens. Matter Mater. Phys.* **2013**, *87*, 235441.
(24) Kamysbayev, V.; Filatov, A. S.; Hu, H.; Rui, X.; Lagunas, F.; Wang, D.; Klie, R. F.; Talapin, D. V. Covalent Surface Modifications and Superconductivity of Two-Dimensional Metal Carbide MXenes. *Science* **2020**, *369*, 979−983.
(25) Morales-García, Á.; Calle-Vallejo, F.; Illas, F. MXenes: New Horizons in Catalysis. *ACS Catal.* **2020**, *10*, 13487−13503.
(26) Li, Z.; Wu, Y. 2D Early Transition Metal Carbides (MXenes) for Catalysis. *Small* **2019**, *15*, 1804736.
(27) Handoko, A. D.; Steinmann, S. N.; Seh, Z. W. Theory-Guided Materials Design: Two-Dimensional MXenes in Electro- and Photocatalysis. *Nanoscale Horiz.* **2019**, *4*, 809−827.
(28) Ran, J.; Gao, G.; Li, F. T.; Ma, T. Y.; Du, A.; Qiao, S. Z. Ti_3C_2 MXene Co-Catalyst on Metal Sulfide Photo-Absorbers for Enhanced Visible-Light Photocatalytic Hydrogen Production. *Nat. Commun.* **2017**, *8*, 13907.
(29) Zhang, X.; Lei, J.; Wu, D.; Zhao, X.; Jing, Y.; Zhou, Z. A Ti-Anchored Ti_2CO_2 Monolayer (MXene) as a Single-Atom Catalyst for CO Oxidation. *J. Mater. Chem. A* **2016**, *4*, 4871−4876.
(30) Zhang, J.; Zhao, Y.; Guo, X.; Chen, C.; Dong, C.-L.; Liu, R.-S.; Han, C.-P. Y.; Li, Y.; Gogotsi, Y.; Wang, G. Single Platinum Atoms Immobilized on an MXene as an Efficient Catalyst for the Hydrogen Evolution Reaction. *Nat. Catal.* **2018**, *1*, 985−992.
(31) Zhao, D.; Chen, Z.; Yang, W.; Liu, S.; Zhang, X.; Yu, Y.; Cheong, W. C.; Zheng, L.; Ren, F.; Ying, G.; Cao, X.; Wang, D.; Peng, Q.; Wang, G.; Chen, C. MXene (Ti_3C_2) Vacancy-Confined Single-Atom Catalyst for Efficient Functionalization of CO_2. *J. Am. Chem. Soc.* **2019**, *141*, 4086−4093.
(32) Zhang, X.; Zhang, Z.; Li, J.; Zhao, X.; Wu, D.; Zhou, Z. Ti_2CO_2 MXene: A Highly Active and Selective Photocatalyst for CO_2 Reduction. *J. Mater. Chem. A* **2017**, *5*, 12899−12903.
(33) Ye, R. P.; Ding, J.; Gong, W.; Argyle, M. D.; Zhong, Q.; Wang, Y.; Russell, C. K.; Xu, Z.; Russell, A. G.; Li, Q.; Fan, M.; Yao, Y. G. CO_2 Hydrogenation to High-Value Products via Heterogeneous Catalysis. *Nat. Commun.* **2019**, *10*, 5698.
(34) International Energy Agency (IEA). *Putting CO_2 to Use*; IEA: Paris, France, 2019
(35) Kresse, G.; Furthmüller, J. Efficient Iterative Scheme for Ab Initio Total-Energy Calculations Using a Plane-Wave Basis Set. *Phys. Rev. B: Condens. Matter Mater. Phys.* **1996**, *54*, 11169.
(36) Perdew, J. P.; Burke, K.; Ernzerhof, M. Generalized Gradient Approximation Made Simple. *Phys. Rev. Lett.* **1996**, *77*, 3865−3868.
(37) Grimme, S.; Antony, J.; Ehrlich, S.; Krieg, S. A Consistent and Accurate Ab Initio Parametrization of Density Functional Dispersion Correction (DFT-D) for the 94 Elements H-Pu. *J. Chem. Phys.* **2010**, *132*, 154104.
(38) Blöch, P. E. Projector augmented-wave method. *Phys. Rev. B* **1994**, *50*, 17953.
(39) Kresse, G.; Joubert, D. From Ultrasoft Pseudopotentials to the Projector Augmented-Wave Method. *Phys. Rev. B: Condens. Matter Mater. Phys.* **1999**, *59*, 1758−1775.
(40) Henkelman, G.; Uberuaga, B. P.; Jónsson, H. A. Climbing Image Nudged Elastic Band Method for Finding Saddle Points and Minimum Energy Paths. *J. Chem. Phys.* **2000**, *113*, 9901.
(41) Henkelman, G.; Jónsson, H. A Dimer Method for Finding Saddle Points on High Dimensional Potential Surfaces Using Only First Derivatives. *J. Chem. Phys.* **1999**, *111*, 7010.
(42) Reuter, K.; Scheffler, M. Composition, Structure, and Stability of $RuO_2(110)$ as a Function of Oxygen Pressure. *Phys. Rev. B* **2002**, *65*, 035406.
(43) Reuter, K.; Scheffler, M. First-Principles Atomistic Thermodynamics for Oxidation Catalysis: Surface Phase Diagrams and Catalytically Interesting Regions. *Phys. Rev. Lett.* **2003**, *90*, 046103.
(44) Posada-Pérez, S.; Viñes, F.; Valero, R.; Rodriguez, J. A.; Illas, F. Adsorption and Dissociation of Molecular Hydrogen on Orthorhombic β-Mo_2C and Cubic δ-MoC (001) Surfaces. *Surf. Sci.* **2017**, *656*, 24−32.
(45) Filot, I. A. W. *Introduction to Microkinetic Modeling*; Technische Universiteit Eindhoven, 2018.
(46) Filot, I. A.W.; Van Santen, R. A.; Hensen, E. J. M. The Optimally Performing Fischer−Tropsch Catalyst. *Angew. Chem., Int. Ed.* **2014**, *53*, 12746−12750.
(47) Zhao, S.; Kang, W.; Xue, J. Manipulation of Electronic and Magnetic Properties of M_2C (M = Hf, Nb, Sc, Ta, Ti, V, Zr) Monolayer by Applying Mechanical Strains. *Appl. Phys. Lett.* **2014**, *104*, 133106.
(48) Wang, G. Theoretical Prediction of the Intrinsic Half-Metallicity in Surface-Oxygen-Passivated Cr_2N MXene. *J. Phys. Chem. C* **2016**, *120*, 18850−18857.
(49) Kumar, H.; Frey, N. C.; Dong, L.; Anasori, B.; Gogotsi, Y.; Shenoy, V. B. Tunable Magnetism and Transport Properties in Nitride MXenes. *ACS Nano* **2017**, *11*, 7648−7655.
(50) He, J.; Lyu, P.; Nachtigall, P. New two-dimensional Mn-based MXenes with Room-Temperature Ferromagnetism and Half-Metallicity. *J. Mater. Chem. C* **2016**, *4*, 11143−11149.

https://doi.org/10.1021/acscatal.1c03150
ACS Catal. 2021, 11, 12850−12857

(51) Terriberry, T. B.; Cox, D. F.; Bowman, D. A. A Tool for the Interactive 3D Visualization of Electronic Structure in Molecules and Solids. *Comput. Chem.* **2002**, *26*, 313−319.
(52) Bader, R. F. W. A Quantum Theory of Molecular Structure and Its Applications. *Chem. Rev.* **1991**, *91*, 893−928.
(53) Zurita, S.; Rubio, J.; Illas, F. Active Sites of Pt Surfaces from Ab Initio Cluster Model Molecular Electrostatic Potential Maps. *Electrochim. Acta* **1996**, *41*, 2275−2283.
(54) López, M.; Broderick, L.; Carey, J. J.; Viñes, F.; Nolan, M.; Illas, F. Tuning Transition Metal Carbide Activity by Surface Metal Alloying: A Case Study on CO_2 Capture and Activation. *Phys. Chem. Chem. Phys.* **2018**, *20*, 22179−22186.
(55) López, M.; Viñes, F.; Nolan, M.; Illas, F. Predicting the Effect of Dopants on CO2 Adsorption in Transition Metal Carbides: Case Study on TiC (001). *J. Phys. Chem. C* **2020**, *124*, 15969−15976.
(56) Seredych, M.; Eugene Shuck, C.; Pinto, D.; Alhabeb, M.; Precetti, E.; Deysher, G.; Anasori, B.; Kurra, N.; Gogotsi, Y. High-Temperature Behavior and Surface Chemistry of Carbide MXenes Studied by Thermal Analysis. *Chem. Mater.* **2019**, *31*, 3324−3332.
(57) Salim, O.; Mahmoud, A. K.; Pant, K. K.; Joshi, R. K. Introduction to MXenes: Synthesis and Characteristics. *Mater. Today Chem.* **2019**, *14*, 100191.
(58) Liu, R.; Li, W. High-Thermal-Stability and High-Thermal-Conductivity $Ti_3C_2T_x$ MXene/Poly(vinyl alcohol) (PVA) Composites. *ACS Omega* **2018**, *3*, 2609−2617.
(59) Xiao, X.; Yu, H.; Jin, H.; Wu, M.; Fang, Y.; Sun, J.; Hu, Z.; Li, T.; Wu, J.; Huang, L.; Gogotsi, Y.; Zhou, J. Salt-Templated Synthesis of 2D Metallic MoN and Other Nitrides. *ACS Nano* **2017**, *11*, 2180−2186.

https://doi.org/10.1021/acscatal.1c03150
ACS Catal. 2021, 11, 12850−12857